A Mouse Model for Sorsby Fundus Dystrophy

Bernhard H. F. Weber,[1] Biaoyang Lin,[1,2] Karen White,[1] Konrad Kohler,[3] Galina Soboleva,[1] Sabine Herterich,[1] Mathias W. Seeliger,[4] Gesine B. Jaissle,[4] Christian Grimm,[5] Charlotte Reme,[5] Andreas Wenzel,[5] Esther Asan,[6] and Heinrich Schrewe[7,8]

Purpose. Sorsby fundus dystrophy (SFD) is a rare, late-onset macular dystrophy caused by mutations in the tissue inhibitor of metalloproteinases-3 (*TIMP3*) gene. The known mutations introduce potentially unpaired cysteine residues in the C terminus of the protein and result in the formation of higher-molecular-weight protein complexes of as yet unknown composition and functional consequences in the pathologic course of SFD. To facilitate in vivo investigation of mutant *TIMP3*, the authors generated a knock-in mouse carrying a disease-related Ser156Cys mutation in the orthologous murine *Timp3* gene.

Methods. Site-directed mutagenesis and homologous recombination in embryonic stem (ES) cells was used to generate mutant ES cells carrying the $Timp3^{S156C}$ allele. Chimeric animals were obtained, of which two displayed germline transmission of the mutated allele. Molecular genetic, biochemical, electron microscopic, and electrodiagnostic techniques were used for characterization.

Results. At 8 months of age, knock-in mice showed abnormalities in the inner aspect of Bruch's membrane and in the organization of the adjacent basal microvilli of the retinal pigment epithelium (RPE). Changes resembling those in the mutant animals were also present to some extent in normal littermates, but only at an advanced age of 30 months. Long-term electrodiagnostic recordings indicated normal retinal function throughout life. The biochemical characteristics of the mutant protein appear similar in humans and knock-in mice, suggesting common molecular pathways in the two species. The localization of the mutant protein in the eye is normal, although there is evidence of increased Timp3 levels in Bruch's membrane of mutant animals.

Conclusions. The knock-in mice display early features of age-related changes in Bruch's membrane and the RPE that may represent the primary clinical manifestations of SFD. In addition, our immunolabeling studies and biochemical data support a model proposing that site-specific excess rather than absence or deficiency of functional Timp3 may be the primary consequence of the known *Timp3* mutations. (*Invest Ophthalmol Vis Sci.* 2002;43:2732–2740)

Sorsby fundus dystrophy (SFD) is a rare hereditary degenerative disease of the retina. The condition generally manifests in the fourth decade of life, with rapid loss of central vision followed by progressive loss of peripheral vision, leading ultimately to blindness.[1] A regular finding is the abnormal deposition of lipofuscin-like material and thickening of Bruch's membrane.[2,3] Over the course of the disease, there is subretinal neovascularization, peripherally extending atrophy of the retinal pigment epithelium, and later atrophy of the choriocapillaris. Despite its rarity, the autosomal dominant SFD has attracted much attention, because the clinical features greatly overlap with those of age-related macular degeneration (AMD), a frequently occurring retinal disease of complex origin accounting for most of the late-onset blindness in individuals in developed countries.[4]

In 1994, affected individuals from two unrelated SFD families were found to harbor heterozygous point mutations in the tissue inhibitor of metalloproteinases-3 (*TIMP3*) gene.[5] TIMP3 is a member of a family of four secreted proteins (TIMP1 to TIMP4) that were originally identified as inhibitors of the matrix metalloproteinases (MMPs),[6] but were recently found also to interact with other members of the zinc-dependent protease (e.g., with a disintegrin and metalloproteinase with thrombospondin motifs ADAM or ADAMTS) family.[7,8] Because the various groups of proteolytic enzymes are involved in the degradation of the extracellular matrix (ECM), the interactions between the TIMPs and the proteases ultimately regulate the composition of the ECM, consequently affecting cell growth and survival, migration, and function.[9,10] Similar to other TIMP proteins, TIMP3 consists of two domains. The N-terminal domain is involved in MMP inhibition, whereas the C-terminal domain binds the ECM.[11] All *TIMP3* mutations described in patients with SFD to date reside in or affect exon 5 of the gene and are predicted to generate unpaired cysteine residues within the C-terminal portion of the protein.[5,12–16] Heterologous expression of mutant TIMP3 in COS7 cells demonstrates that at least three of these mutations result in proteins that retain inhibitory activity and localize to the ECM but form high-molecular-weight complexes, the nature and consequences of which have not yet been established.[11,16]

A better understanding of the biological role of mutant TIMP3 in SFD would be greatly facilitated by the use of a model experimental system. We report the generation of mice carrying a *Timp3* alteration orthologous to a mutation found in a large SFD pedigree.[12]

Materials and Methods

Site-Directed Mutagenesis and Construction of a Targeting Vector

Recombinant phage clones containing the *Timp3* locus were isolated from a 129/SvJ mouse genomic DNA library constructed in lambda FIX II (Stratagene, La Jolla, CA). The Ser156Cys mutation was introduced

From the [1]Institute of Human Genetics, Biocenter, University of Wuerzburg, Germany; the [2]Institute for Systems Biology, Seattle, Washington; the [3]Department of Experimental Ophthalmology and the [4]Retinal Electrodiagnostics Research Group, Department of Pathophysiology of Vision and Neuroophthalmology, University Eye Hospital, Tübingen, Germany; the [5]Eye Clinic, University Hospital, Zürich, Switzerland; the [6]Institute of Anatomy, University of Wuerzburg, Germany; the [7]School of Biosciences, The University of Birmingham, Birmingham, United Kingdom; and the [8]Department of Developmental Biology, Max-Planck-Institute for Immune Biology, Freiburg, Germany.

Supported by grants from the Ernst and Berta Grimmke-Stiftung Düsseldorf, the Swiss National Science Foundation, and the German Research Foundation, Bonn (SFB581, project TB13, and Se837-1/1).

Submitted for publication September 26, 2001; revised March 20, 2002; accepted April 25, 2002.

Commercial relationships policy: N.

The publication costs of this article were defrayed in part by page charge payment. This article must therefore be marked "*advertisement*" in accordance with 18 U.S.C. §1734 solely to indicate this fact.

Corresponding author: Bernhard H. F. Weber, Institute of Human Genetics, Biozentrum, Am-Hubland, D-97074 Wuerzburg, Germany; bweb@biozentrum.uni-wuerzburg.de.

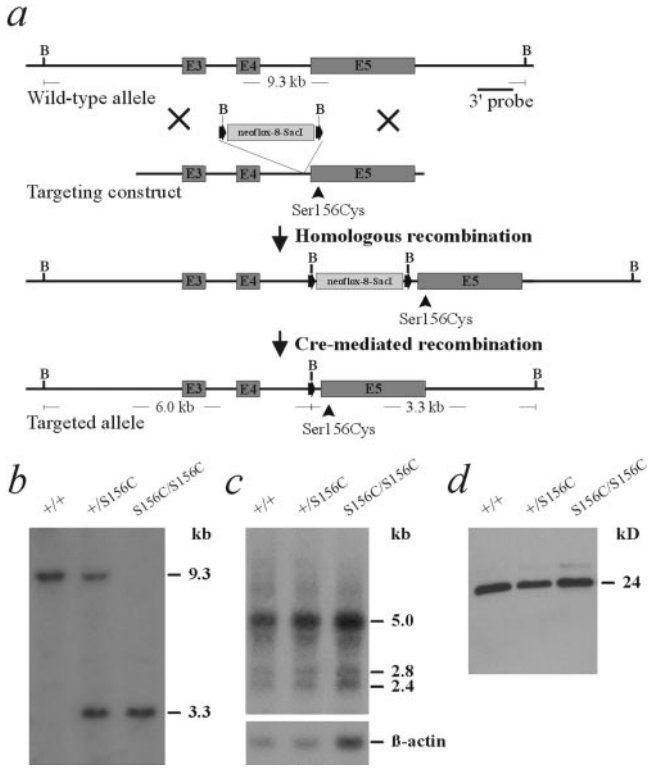

FIGURE 1. Introduction of the Ser156Cys mutation into the mouse *Timp3* locus. (**a**) Targeting construct and predicted structure of the targeted allele. The Ser156Cys mutation in exon 5 was cotransferred with the *neo*^{r} gene (inserted into intron 4 of *Timp3* close to the acceptor splice site of exon 5 flanked by *loxP* sites) through homologous recombination in ES cells. Before microinjection into C57BL/6 blastocysts, targeted ES cells were treated in culture with Cre recombinase to excise the *neo*^{r} gene. B, *Bam*HI, E3 to E5 corresponds to exons 3 to 5 of *Timp3.* (**b**) Southern blot analysis of *Bam*HI-digested DNA isolated from wild-type (+/+), heterozygous (+/S156C), and homozygous (S156C/S156C) mice, demonstrating the accuracy of the targeting event by the presence of a 3.3-kb *Bam*HI fragment after hybridization with the external 3′ probe. (**c**) Northern blot analysis of total kidney RNA reveals the presence of the three known isoforms of *Timp3* in wild-type, *Timp3*$^{+/S156C}$, and *Timp3*$^{S156C/S156C}$ mice. The filter was reprobed with β-actin to test for RNA integrity and loading (**d**) Western blot analysis of ECM protein extracts obtained from fibroblast cultures of wild type, *Timp3*$^{+/S156C}$, and *Timp3*$^{S156C/S156C}$ mice using murine antibody pmAB#50. The Timp3 protein was present in wild type and ECM preparations from heterozygous and homozygous fibroblast cell lines.

into a 2.7-kb *Hinc*II fragment with PCR primers mutl56bom (5′-GGC GTA GTG TTT GCA CTG ATA GCC AGG GTA CCC-3′) and mut156top (5′-GGG TAC CCT GGC TAT CAG TGC AAA CAC TAC GCC-3′). Similarly, an artificial *Sac*I site was generated in intron 4 of *Timp3* with primers MutSacI (5′-GCC TGC CAT GGT GAG CTC CCC TAA CTG TGG C-3′) and MutSac2 (5′-GCC ACA GTT AGG GGA GCT CAC CAT GGC AGG C-3′). Ligation of restriction fragments *Xba*I-*Hinc*II (1.3 kb), *Hinc*II-*Sac*I (1.7 kb), *Sac*I/*Sac*I neoflox-8-*Sac*I (1.3 kb), and *Sac*I-*Sph*I (1.3 kb) resulted in the final targeting construct (Fig. 1a). Linearization of the plasmid was achieved with *Sfi*I.

Homologous Recombination in ES Cells and Generation of Germline Chimeras

After G418 selection, 400 ES clones were analyzed by Southern hybridization of *Bam*HI-digested DNA to a 3′ external probe (Figs. 1a, 1b). Cre recombinase was transiently expressed in two targeted ES cell lines to mediate excision of the *loxP* flanked *neo*^{r} cassette. Mutant ES cells carrying the *Timp3*^{S156C} allele were injected into C57BL/6 blastocysts, as described.[17] Two male chimeras (numbers 15 and 17) were bred to C57BL/6 females to test for germ line transmission. F1 and F2 progenies of 129/Sv and hybrid C57BL/6 × 129/SvJ background were further analyzed. All experimental procedures were conducted according to the ARVO Statement for the Use of Animals in Ophthalmic and Vision Research.

Northern Blot Analysis and RT-PCR

Total RNA isolation from mouse eyecup and kidney and Northern blot analysis were performed as described.[18] The hybridization probe encompasses the coding sequence of mouse *Timp3* and was generated by RT-PCR with primers muTimp3for (5′-GGC TCT TCC ATG ACT CCC TGG CTT GGG CTT-3′) and muTimp3rev (5′-TGC TCT TCG AAG CTA TCA GGG GTC TGT GGC GTT-3′). Sequencing of the wild-type and mutant murine *Timp3* exon 5 was done with primers mTimp3_ex5F (5′-TGC AAG ATC AAG TCC TGC T-3′) and mTimp3_ex5R (5′-GGT GAG GTG GGG CAG GTC T-3′).

SDS-Polyacrylamide Gel Electrophoresis, Western Blot Analysis, and Immunofluorescence Labeling

Eyecups were homogenized in PBS buffer. Quantitation of protein extracts was performed by Coomassie staining and subsequent visual inspection or by the protein assay based on the method of Bradford (Bio-Rad Laboratories, Munich, Germany; Ref. 19). Extracellular matrix was isolated from fibroblast cell cultures of patients with SFD carrying a heterozygous Ser156Cys[12] or Ser181Cys[5] *TIMP3* mutation or from *Timp3*$^{+/+}$, *Timp3*$^{+/S156C}$, and *Timp3*$^{S156C/S156C}$ mice after removal of cells with trypsin, washing in PBS buffer containing phenylmethylsulfonyl fluoride (PMSF; 80 μg/mL) and β-caproic acid (1 mg/mL) and dissolving in ECM buffer (100 mM Tris-HCl [pH 6.8], 10% glycerin, and 1% SDS). Protein samples were added to a 1:1 volume of a solution containing 125 mM Tris-HCl (pH 6.8), 2% SDS, 10% sucrose, 0.02% bromophenol blue in the presence or absence of 5% β-mercaptoethanol (β-ME).

For immunodetection, 16-amino-acid peptides (human: RGWAPPDKSIINATDP; mouse: RGWAPPDKSISNATDP) corresponding to amino acids 196-211 of human and mouse TIMP3 were conjugated to keyhole limpet hemocyanin and used to immunize New Zealand White rabbits (human: phAB#57; mouse: pmAB#50). The polyclonal antibodies were purified on a protein A affinity column and used in a 1:1000 dilution. In addition, polyclonal rabbit antisera directed against RPE-specific protein, 65 kDa (RPE65),[20] interphotoreceptor retinoid-binding protein (IRBP),[21] cellular retinaldehyde-binding protein (CRALBP),[22] and arrestin[23] were used.

For immunofluorescence labeling, retinal sections were mounted (Tissue-Tek 4583; Sakura Finetek Europe, Zoeterwoude, The Netherlands), cryosectioned (12 μm), and collected on polylysine-treated slides. The sections were incubated with the primary antibody for 2 hours at 37°C. The control sections were labeled with the same antibody but in the presence of the 16-amino-acid Timp3 peptide antigen (100 μg/mL). The sections were washed in PBS buffer containing 0.05% Tween 20. The secondary antibody (swine anti-rabbit FITC-labeled; Dako A/S, Glostrup, Denmark) was used in a dilution of 1:1000. The sections were incubated for 1 hour at 37°C, washed in PBS buffer containing 0.05% Tween 20, mounted in antifade medium (Vectashield; Vector Laboratories, Burlingame, CA) and analyzed using fluorescence microscopy (Carl Zeiss, Oberkochen, Germany).

Scanning Laser Ophthalmoscopy

Fundus imaging was performed with scanning laser ophthalmoscopy (SLO) using a scanning frequency of 50 Hz and an infrared wavelength of 780 nm (Rodenstock Instruments, Düsseldorf, Germany). A standard 20-D ophthalmoscope lens (Volk Optical, Mentor, OH) was inserted in the optical pathway between the SLO and the eye.[24,25] The confocal diaphragm of the SLO facilitates imaging in different planes of the

posterior pole which can be viewed sequentially by varying the focus from +15 D (surface) to +5 D (RPE).

Electroretinography

ERGs were obtained according to previously described procedures.[26] In brief, mice were dark-adapted overnight (at least 6 hours) before the experiments and their pupils dilated. They were anesthetized by subcutaneous injection of ketamine (66.7 mg/kg), xylazine (11.7 mg/kg), and atropine (1 mg/kg). Silver needle electrodes served as reference (forehead) and ground (tail), and rings made from 0.5 mm^2 gold wire served as monopolar corneal electrodes. ERGs were recorded from both eyes simultaneously. Band-pass filter cutoff frequencies were 0.3 and 300 Hz. Single-flash recordings were obtained both under dark-adapted (scotopic) and light-adapted (photopic) conditions. Light adaptation before the photopic session was achieved with a background illumination of 30 cd/m^2 presented for 10 minutes. Flash stimulus intensities were increased under scotopic conditions from 10^{-4} cd/sec · m^2 to 25 cd/sec · m^2, divided into 10 steps of 0.5 and 1 log cd/sec · m^2, and under photopic conditions from 10^{-3} cd/sec · m^2 to 25 cd/sec · m^2, divided into seven steps of 0.5 and 1 log cd/sec · m^2. Ten subsequent responses were averaged with an interstimulus interval (ISI) of 5 or 17 seconds (for 1, 3, 10, and 25 cd/sec · m^2).

Electron Microscopy

For electron microscopy, light-adapted eyes were enucleated and hemisected along the ora serrata. The posterior eyecups were immediately immersed overnight in ice-cold fixative (1% paraformaldehyde, 2.5% glutaraldehyde in 0.05 M phosphate buffer, [pH 7.2]). Retinas were washed, postfixed in 1% osmium, en bloc-stained in 2% uranyl acetate, dehydrated in graded acetone and embedded in resin (Taab Laboratories, Aldermaston, UK).

Light Damage and Rhodopsin Regeneration

Timp3$^{S156C/S156C}$ mice between 6 and 12 weeks of age were dark adapted and subsequently exposed to diffuse white fluorescent light for 2 hours with an intensity of 5,000 or 15,000 lux. Animals were analyzed after a 24-hour period in darkness or after 14 days in the light–dark cycle. Bleaching of rhodopsin was achieved by exposing dark-adapted mice for 10 minutes to 5,000 lux of white light. Light was switched off to allow metabolic rhodopsin regeneration in darkness. Rhodopsin levels were determined as described.[23]

PCR Amplification and Sequence Determination of RPE65

DNA was prepared from tail biopsy specimens and amplified with primer pair RPE65/450A (5′-ATA TTA AAT CAG CTC TGT AAG A-3′) and RPE65/450Rev (5′-CAT TAC CAT CAT CTT CTT CCA-3′) or with primer pair RPE65/450C (5′-ATA TTA AAT CAG CTC TGT AAG C-3′) and RPE65/450Rev. The first primer pair results in an amplicon of 150 bp when the substrate DNA encodes Met but not Leu at codon 450 of *RPE65*. When a Leu is encoded at this position, PCR with primer pair 2 but not primer pair 1 results in the appropriate product.

Disc Shedding

Mice were kept individually in cages in a normal 12:12-hour light–dark cycle (60 lux at cage level). Pupils were dilated as described earlier and mice exposed to 13,000 lux for 1 hour at the beginning of the light cycle. Retinal tissue was isolated after a 90-minute recovery period in darkness and prepared for light microscopy, as described earlier. Phagosomes were counted in 10 consecutive fields of 180 μm length, and the numbers were averaged. Means of six retinas were statistically analyzed by an unpaired *t*-test.

Results

Generation of *Timp3*$^{+/S156C}$ Knock-in Mice

A construct containing the Ser156Cys mutation was generated using site-directed mutagenesis and targeted into the murine *Timp3* locus through homologous recombination in ES cells (Fig. 1a). In positive lines Cre recombinase was transiently expressed to excise the *neo*^{r} cassette and mutant ES cells were microinjected into C57BL/6 blastocysts, yielding two high-percentage chimeric males. Progeny of 129/Sv and hybrid C57BL/6x129/Sv background were assessed for genotype and manifestation of the SFD phenotype. Germline transmission of the correctly targeted *Timp3*^{S156C} allele was confirmed by the detection of a 3.3- and a 6.0-kb *Bam*HI fragment in Southern hybridizations (Figs. 1a, 1b and data not shown). RNA isolated from kidney tissue that is known to express Timp3 abundantly in adult mice,[27] was analyzed by Northern blot analysis, detecting the correct transcript sizes of the three known Timp3 isoforms in wild-type, heterozygous *Timp3*$^{+/S156C}$, and homozygous *Timp3*$^{S156C/S156C}$ mice (Fig. 1c). In addition, sequencing of RT-PCR products from eyecup total RNA with primers flanking the S156C mutation in exon 5 of *Timp3* demonstrated transcription of the *Timp3*^{S156C} allele in both heterozygous and homozygous mice (data not shown). Expression of the Timp3 protein was confirmed by Western blot analysis of extracellular matrix extracts from fibroblast cultures derived from wild-type, *Timp3*$^{+/S156C}$, and *Timp3*$^{S156C/S156C}$ mice (Fig. 1d).

Scanning-Laser Ophthalmoscopy and Electroretinography

Sequential SLO was performed in two 14-month-old *Timp3*$^{+/S156C}$ mice and, for comparison, in two wild-type animals (Fig. 2a). Analyses of the various planes of the posterior pole, from the surface of the retina down to the RPE, did not reveal any morphologic abnormalities in the *Timp3*$^{+/S156C}$ mice. ERG Ganzfeld examinations of five wild-type and six *Timp3*$^{+/S156C}$ mice showed no differences in either waveform shape or signal amplitude over the entire intensity range (Fig. 2b and data not shown). The scotopic and photopic b-wave amplitudes were recorded over a period of 2 years in four mutant and four wild-type eyes, respectively (Fig. 2c). Although there was a general decrease in amplitude over time in both mutant and control animals, there was no sign of impaired retinal function in *Timp3*$^{+/S156C}$ mice at any age.

Electron Microscopic Analysis of the Retinal Pigment Epithelium, Bruch's Membrane, and the Retina

For comparison of the ultrastructure, two animals each from wild-type, heterozygous *Timp3*$^{+/S156C}$ and homozygous *Timp3*$^{S156C/S156C}$ mice were analyzed at the ages of 8 and 30 months, respectively. In both age groups, electron microscopy revealed no alterations between wild-type and mutant mice in the neuronal layers of the retina, including the inner nuclear and ganglion cell layers and the photoreceptor inner and outer segments.

In 8-month-old wild-type animals, the RPE showed no structural abnormalities (Figs. 3a–c). The apical processes of the RPE cells were vertically and regularly aligned and in close contact with the adjacent photoreceptor outer segments. The labyrinth of the basal microvilli was compact and dense (Fig. 3c). In the *Timp3*$^{+/S156C}$ mice, no alterations in the appearance of the apical processes were observed in the major parts of our electron microscopy specimen. In some areas (15%–20% of areas analyzed), however, the vertical orientation was less

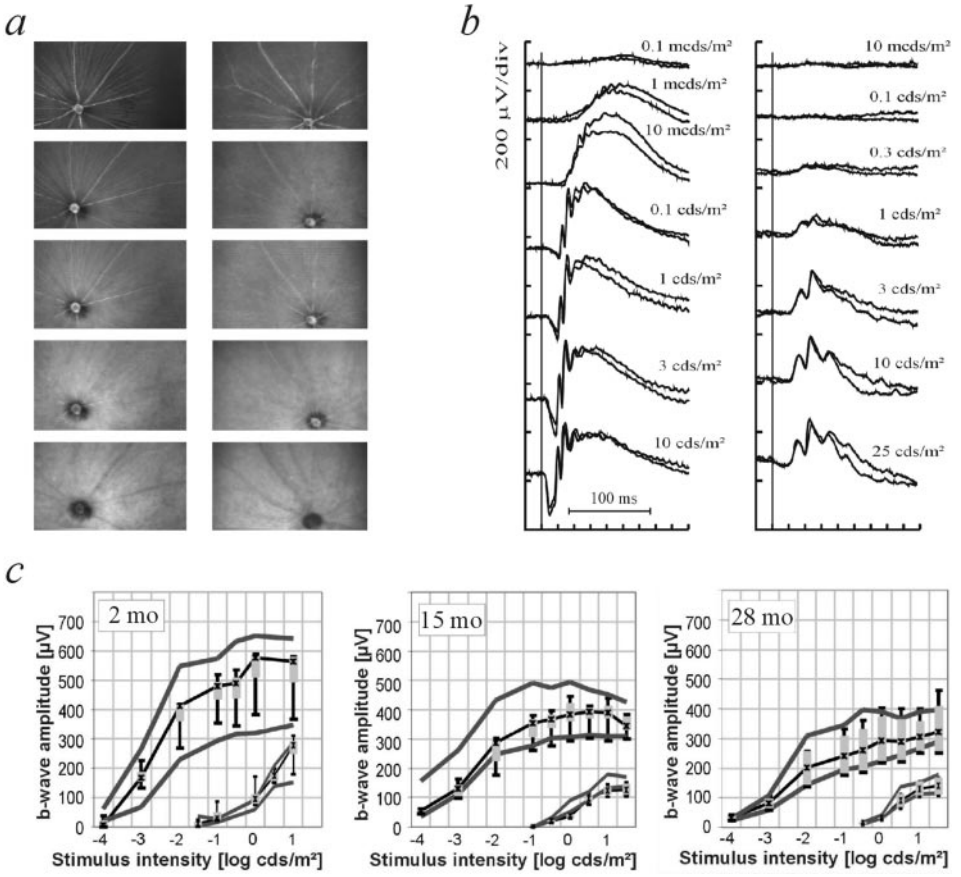

FIGURE 2. Macromorphologic and electrophysiological evaluation of *Timp3*$^{+/S156C}$ mice. (**a**) Shown is a representative sequence of images obtained while adjusting the focus from the retinal view (*top row*) down to the RPE view (*bottom row*). There was no macroscopic sign of pathologic retinal morphology in *Timp3*$^{+/S156C}$ mice (*left column*) compared with control animals (*right column*). (**b**) Superposition of the dark-adapted (scotopic, *left column*) and light-adapted (photopic, *right column*) intensity series in a *Timp3*$^{+/S156C}$ and a wild-type mouse. No waveform differences were observed between control and mutant mice. (**c**) Age-related changes of scotopic (*top traces*) and photopic (*bottom traces*) b-wave amplitudes in *Timp3*$^{+/S156C}$ mice up to 28 months of age. *Boxes*: 25% to 75% quantile range; *small crosses*: the median of the *Timp3*$^{+/S156C}$ data. *Solid lines*: normal range is indicated by the 5% and 95% quantiles of the control group. In comparison to the age-matched control animals, there was no sign of impaired retinal function in *Timp3*$^{+/S156C}$ mice at any age.

strict and the distance between processes was increased at the cellular bases (Fig. 3d). Next to Bruch's membrane, a patchy thinning of the layer of the basal microvilli was observed (Figs. 3e, 3f). In addition, the compact packing of the basal microvilli was impaired and occasionally wide-open caverns extended from the basal labyrinth into the cytoplasm of the cell (Figs. 3d–f). The thickness of Bruch's membrane was in the general range of 0.5 and 0.7 μm. There was no significant difference between wild-type and *Timp3*$^{+/S156C}$ or *Timp3*$^{S156C/S156C}$ mice (Figs. 3c, 3f, 3i). In the 8-month-old homozygous *Timp3*$^{S156C/S156C}$ mice, the RPE processes facing the outer segments of the photoreceptors were short and not vertically elongated, but horizontally aligned near the cell bodies of the RPE. Toward the photoreceptors, they were composed of small, vesiculated structures that do not envelop the outer segments (Fig. 3g). In areas where such abnormalities were present, these vesiculated processes seemed to form a barrier between the outer segments and the RPE. Moreover, severe changes in thickness and compactness of the basal microvilli appeared in the *Timp3*$^{S156C/S156C}$ mice. There was a general derangement of the basal layer, with a loss of the palisade-like orientation of the microvilli accompanied by a marked reduction in thickness (Fig. 3h) up to virtually a complete loss of the entire labyrinth (Fig. 3i).

In 30-month-old control animals, the five-layered structure of Bruch's membrane was clearly visible (Figs. 4a–d), although there was a general tendency of the thickness of the membrane to be in the upper range of 0.8 μm (Fig. 4b). The width of the basal labyrinth was greatly reduced in these animals compared with that in the 8-month-old wild-type mice. In some areas the basal microvilli of the aged control animals were absent (Fig. 4d), resembling the findings in the 8-month-old homozygous *Timp3*$^{S156C/S156C}$ mice (Fig. 3i). In both heterozygous and homozygous 30-month-old mutant animals (Figs. 4e–l) the layering of Bruch's membrane was still present (Figs. 4e, 4i) but less clearly expressed, and a higher amount of granular debris was accumulating in the inner layers of the extracellular membrane (Figs. 4f, 4g, 4j). The overall thickness of Bruch's membrane varied from 0.5 (Fig. 4e) to 1.2 μm (Fig. 4j). Similar to the aged wild-type animals a layer of electron dense material occurred proximal to the basement membrane in the heterozygous mice (Figs. 4c, 4g, stars), although this layer was generally more pronounced in the mutant animals (Figs. 4h, 4k, stars) and in some instances reached into the soma of the RPE (Fig. 4k, asterisk). In areas where the microvilli labyrinth was completely lost the soma of the RPE was interspersed with large caverns (Fig. 4l).

Western Blot Analysis

To test for altered levels of a selected number of retina and RPE proteins, eyecup protein extracts were assayed with antibodies directed against IRBP, RPE65, arrestin, and CRALBP. Similar levels of protein were found in *Timp3*$^{S156C/S156C}$ and wild-type mice (Fig. 5a).

Western blot analyses under nonreducing conditions (without β-ME) of extracellular matrix extracts derived from fibroblast cultures from patients with SFD carrying a heterozygous Ser156Cys or a Ser181Cys mutation demonstrate the occurrence of higher-molecular-weight complexes specifically labeled by the human peptide antibody phAB#57 (Fig. 5b). Protein extracts from murine *Timp3*$^{S156C/S156C}$ fibroblast cell line ECM behave similarly and label higher-molecular-weight complexes under nonreducing, but not under reducing, conditions (Fig. 5b). In protein extracts from the RPE-choroid of homozygous mice higher-molecular-weight complexes of similar molecular weight (approximately 40–45 kDa) compared with the ECM extracts are present (Fig. 5c). To test for Timp3

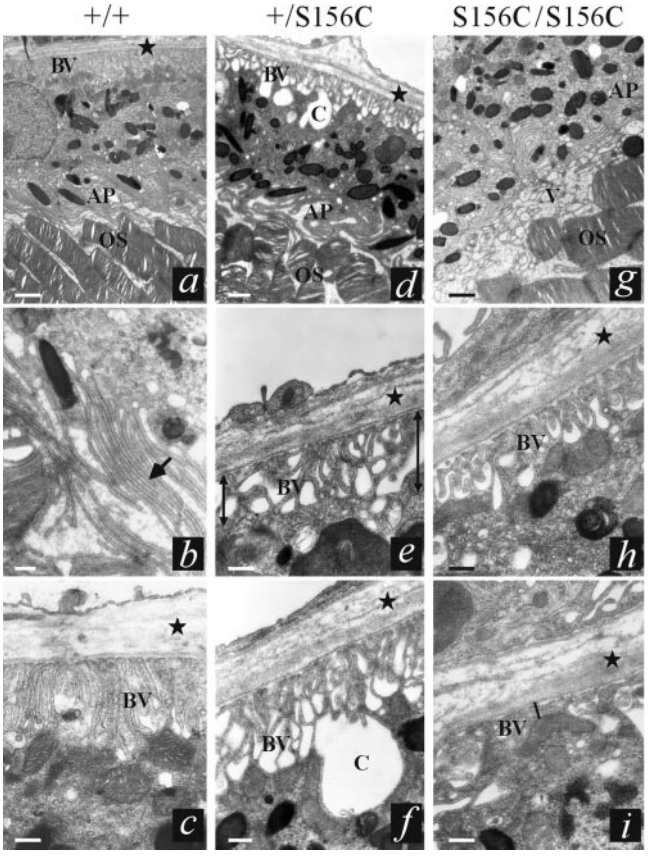

FIGURE 3. Electron photomicrographs of 8-month-old *Timp3*$^{+/+}$, *Timp3*$^{+/S156C}$, and *Timp3*$^{S156C/S156C}$ mice. (**a–c**) Wild-type mice showed a normally developed RPE with elongated apical processes (**b**; *arrow*) and a compact layer of basal microvilli (**c**). (**d–f**) Heterozygous *Timp3*$^{+/S156C}$ mice displayed localized disorientation of the apical processes and reduction in thickness (**e**; marked with *vertical lines*) and complexity (**e**, **f**) of the basal microvilli. Occasionally, caverns protruded into the cytoplasm (**f**). (**g–i**) In *Timp3*$^{S156C/S156C}$ mice, the elongation of the apical processes was disturbed, and the processes were vesiculated toward the outer segments. The arrangement of the basal microvilli was severely damaged (**h**) up to nearly a complete loss of the basal structure (**i**). (⋆) Bruch's membrane. AP, apical processes; BV, basal microvilli; C, cavern; OS, outer segments; V, vesiculated processes. Bar: (**a**, **d**, **g**) 1.0 μm; (**b**, **c**, **e**, **f**, **h**, **i**) 0.5 μm.

levels in normal and homozygous knock-in mice, serial dilutions of total protein extracts from RPE-choroid were labeled with murine Timp3 antibody pmAB#50 (Fig. 5d). At 20 μg of total protein extracts, Timp3 was only weakly labeled in the wild-type sample, whereas there was a stronger immunoreaction in the mutant sample. Immunoreactivity was still observed at 10 μg of protein extracts in the mutant but not in the control tissue.

Localization of Normal and Mutant Timp3 in the Mouse Retina

To determine Timp3 localization in the normal and mutant mouse retina, immunofluorescence labeling of *Timp3*$^{+/+}$ and *Timp3*$^{S156C/S156C}$ retinal sections with polyclonal antibody pmAB#50 were performed (Figs. 6a, 6c). Prominent labeling of Bruch's membrane was observed in wild-type and homozygous *Timp3*$^{S156C/S156C}$ retinas. There was also specific labeling of the sclera and minor staining of the photoreceptor outer and inner segments in both wild-type and mutant retinal sections (Figs. 6a, 6c). The specificity of Timp3 immunolabeling was demonstrated by addition of excess of Timp3 peptide antigen during the labeling procedure, which completely abolished immunopositivity of Bruch's membrane and sclera, as well as the minor site of labeling in the photoreceptor layer (Fig. 6b). Similarly, in control studies with rabbit preimmune serum, no immunolabeling was present in mouse retinal sections (data not shown).

Effects of Light Exposure, Rhodopsin Regeneration, and Disc Shedding

To assess the influence of the *Timp3* mutation on retinal light damage susceptibility, we exposed *Timp3*$^{S156C/S156C}$ and wild-type mice to intense white light for 2 hours. Illumination with 5000 lux resulted in the abundant formation of pyknotic nuclei and of apoptotic bodies in retinas of both mutant and wild-type mice compared with dark-adapted control mice (Figs. 7b, 7f). No differences were detected in the susceptibility to light damage between wild-type and mutant retinas. A three times higher dose of light (15,000 lux for 2 hours) increased the signs of cell death with severely disrupted rod inner (RIS) and rod

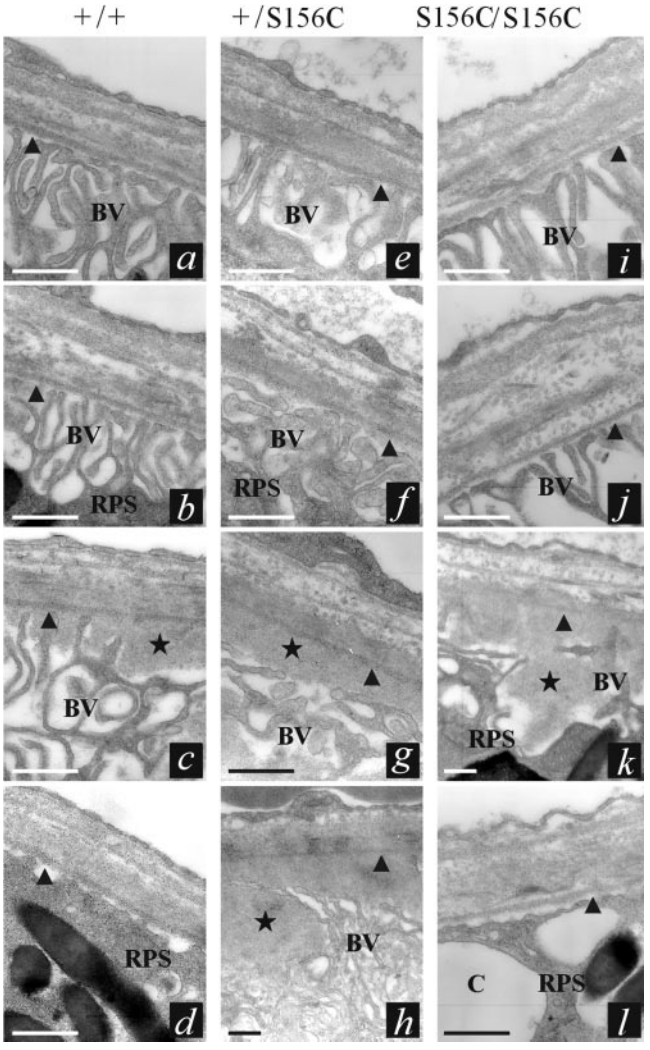

FIGURE 4. Electron photomicrographs of the basal RPE labyrinth and Bruch's membrane in 30-month-old *Timp3*$^{+/+}$ (**a–d**), *Timp3*$^{+/S156C}$ (**e–h**), and *Timp3*$^{S156C/S156C}$ (**i–l**) mice. *Arrowhead*: basement membrane; (⋆) electron-dense material proximal to the basement membrane. BV, basal microvilli; RPS, soma of the retinal pigment epithelium; C, cavern. Bar, 0.5 μm.

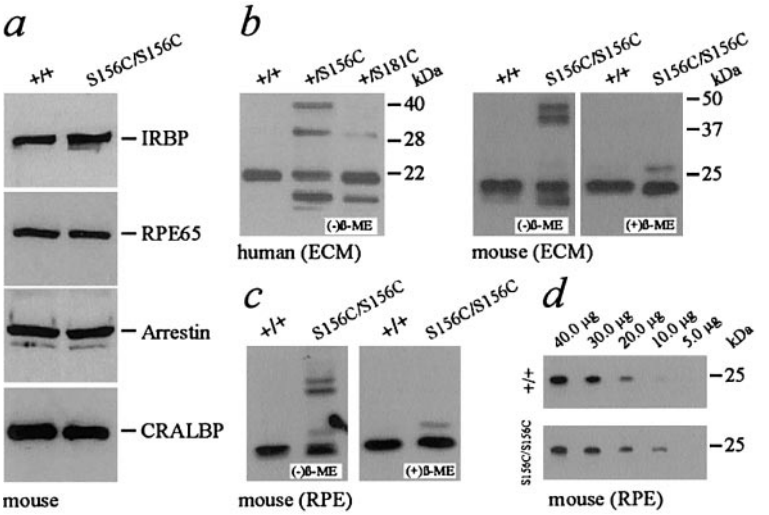

FIGURE 5. Western blot analyses of normal and mutant TIMP3**.** (**a**) Protein levels were similar in wild-type and *Timp3*$^{S156C/S156C}$ mice. Total eyecup protein homogenates were assayed for levels of IRBP, RPE65, arrestin, and CRALBP. (**b**) Under nonreducing conditions, (−)β-ME, additional higher-molecular-weight complexes of *TIMP3* were seen in ECM extracts from fibroblast cultures of patients with SFD carrying heterozygously the Ser156Cys or Ser181Cys mutation but not in control individuals (+/+). The phAB#57 antibody was used. Similar protein complexes were present in ECM preparations of homozygous mice under nonreducing conditions, whereas under reducing conditions, (+)β-ME, these complexes did not form. The pmAB#50 antibody was used. Note the noncomplexed mutant Timp3 in the homozygous *Timp3*$^{S156C/S156C}$ protein extracts under nonreducing conditions, suggesting that not all mutant Timp3 participates in the formation of the higher-molecular-weight complexes. (**c**) Protein preparations from RPE-choroid tissue of wild-type (+/+) and homozygous knock-in mice were electrophoretically separated under reducing and nonreducing conditions. Similar to the results in ECM preparations, higher-molecular-weight complexes of *Timp3* were formed under nonreducing conditions in the *Timp3*$^{S156C/S156C}$ protein extracts. The pmAB#50 antibody was used. (**d**) Total protein extracts from RPE-choroid tissue of wild-type (+/+) and homozygous knock-in mice (S156C/S156C) were serially diluted as indicated and labeled with murine antibody pmAB#50. Note the immunoreactivity at a total protein concentration of 20 µg and 10 µg in the mutant preparations compared with the wild-type.

outer segments (ROS; Figs. 7c, 7g). Fourteen days after the exposure to 15,000 lux for 2 hours, the outer nuclear layer was severely thinned and consisted of approximately one third of the number of cells compared with the unexposed control. ROS and RIS were almost completely absent (Figs. 7d, 7h).

Because susceptibility to light damage is at least partially determined by the rate of rhodopsin regeneration in the visual cycle[28] and because the visual cycle may be influenced by the composition and function of the extracellular matrix, we assessed the rate of rhodopsin regeneration in *Timp3*$^{S156C/S156C}$ mice. The regeneration rate in the visual cycle correlates with the amino acid sequence of the RPE65 protein at position 450. A leucine at this position, as found, for example, in BALB/c mice, led to a fast regeneration with a rate constant of approximately 0.036/minute and, accordingly, to a high susceptibility to light damage. In contrast, C57BL/6 mice, which have a methionine at position 450 of the RPE65 protein, regenerate rhodopsin four times slower, with a rate constant of 0.009/minute, and have a low susceptibility to light damage.[28] We determined the DNA sequence of RPE65 in the *Timp3*$^{S156C/S156C}$ mice. All mice tested ($n = 4$) had a leucine at position 450 in the RPE65 protein. Conformably, the mice regenerated rhodopsin with a rate constant of approximately 0.033/minute (Table 1) indicating that the *Timp3* mutation did not significantly influence regeneration of metabolic rhodopsin.

We also tested the influence of the mutation on light-elicited disc shedding. *Timp3*$^{S156C/S156C}$ mice were raised in a 12:12-hour light–dark cycle with 60 lux at cage level in separate cages for 10 days. Ninety minutes after light exposure to 13,000 lux for 1 hour, retinas were prepared and examined for disc shedding. This treatment resulted in the dilation of ROS (asterisk in Figs. 8b, 8c) and in a burst of disc shedding.[29] The shed material was phagocytosed by the RPE which led to an increase of phagosomes when compared with dark-adapted control retinas (Figs. 8a–c, arrows). The *Timp3* mutation did

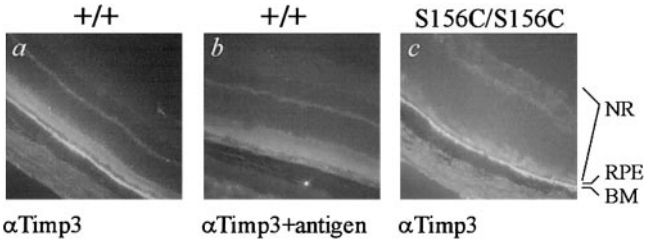

FIGURE 6. Immunofluorescence microscopy of Timp3 in retinal sections from 7-month-old wild-type (+/+) and homozygous (S156C/S156C) mice. (**a**) Intense Timp3 immunolabeling of Bruch's membrane in wild-type. Some minor labeling was also present in the photoreceptor layer and the choroid. (**b**) Control, Timp3 immunolabeling in the presence of excess competing Timp3 peptide. (**c**) Timp3 immunolabling of a homozygous retinal section. Note the intense staining of Bruch's membrane similar to wild-type retina. NR, neuronal retina; RPE, retinal pigment epithelium; BM, Bruch's membrane.

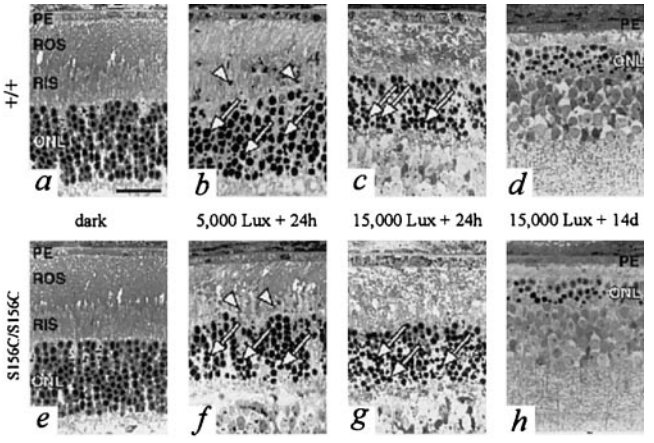

FIGURE 7. Light damage analysis. Wild-type (**a**–**d**) or *Timp3*$^{S156C/S156C}$ mice (**e**–**h**) were kept in darkness (**a**, **e**) or were exposed to 5,000 lux (**b**, **f**) or 15,000 lux (**c**, **d**, **g**, **h**) of white light. After exposure, animals were analyzed after 24 hours in darkness (**b**, **c**, **f**, **g**) or after a 24 hours in darkness followed by a 14-day period in normal cyclic light (**d**, **h**). *Arrows*: samples of pyknotic nuclei. *Arrowheads*: apoptotic bodies; PE, pigment epithelium; ROS, rod outer segments; RIS, rod inner segments; ONL, outer nuclear layer. Bar, 25 µm.

TABLE 1. Rhodopsin Regeneration in *Timp3*$^{S156C/S156C}$ Mice

Condition*	Rhodopsin (nmol, OD/OS)†	Average (% of maximum)	Comment
Dark	0.433/0.460	0.447 (100)	Maximum value; dark adaption for 16 hours
Immediately after illumination	0.067	0.067 (15)	Illumination with 5000 1ux for 10 minutes (standard protocol for bleaching)
Regeneration			
5 minutes	0.075/0.100	0.088 (20)	After bleach, mice recovered in dark for 5 minutes before sample preparation
15 minutes	0.192/0.210	0.201 (45)	After bleach, mice recovered in dark for 15 minutes before sample preparation
30 minutes	0.267/0.330	0.299 (67)	After bleach, mice recovered in dark for 30 minutes before sample preparation

* At time of sample preparation.

† Rate constant for rhodopsin regeneration is approximately 0.033/min and thus very similar to BALB/c mice.[28]

not influence disc shedding and phagocytosis, as judged from similar numbers of phagosomes ($P > 0.3$, unpaired *t*-test, $n = 6$) in the RPE of wild-type (10.1 ± 2.5 phagosomes/180 μm) and *Timp3*$^{S156C/S156C}$ mice (8.8 ± 2.1 phagosomes/180 μm).

DISCUSSION

Elucidation of the mechanisms of human retinal disease has been hampered by the scarcity of diseased material for morphologic and functional studies, as well as by the availability of such material only at advanced stages of the disease, when the primary events of pathogenesis are likely to be obscured. Recent advances allowing the generation of mouse models for retinal disease have helped to overcome these obstacles and facilitate the detailed analysis of the primary retinal disease. With the goal of creating a mouse model for SFD, we have used a gene-targeting strategy to create knock-in mice carrying a Ser156Cys mutation in the endogenous murine *Timp3* gene. This mutation is homologous to one initially identified in a large German-Czech SFD pedigree with onset of symptoms in affected individuals generally in their early 30s.[12]

Patients with SFD with heterozygous mutations in the *TIMP3* gene typically experience loss of central vision in midlife, with ocular examination showing disciform scars of the macula due to neovascularization and atrophy. Progressive atrophy leads to later loss of peripheral vision. The Ganzfeld ERG, which is a valuable indicator of retinal function below the ganglion cell level, may initially be normal in patients with SFD, but usually becomes subnormal in more advanced stages of the disease.[13] Variability in phenotype has been reported, with some patients showing significantly later onset, preservation of the peripheral retina, and normal ERGs.[15] ERGs recorded in heterozygous and homozygous *Timp3* knock-in mice under scotopic and photopic conditions indicate that retinal function is not affected by the presence of mutated *Timp3* during the life span of mice. Similarly, the macromorphologic in vivo analysis using SLO did not reveal any gross abnormalities; in particular, there were no signs of the secondary fundus complications that are usually observed in advanced stages of human disease.

There are few reports on the histopathology of SFD in humans.[2,3,30] Using light and electron microscopy Capon et al.[2] and Chong et al.[3] have described morphologically similar deposits of granular–floccular material between the basement membrane of the RPE and the inner collagenous layer of Bruch's membrane. In the elastic layer, they noted irregularities such as breaks and thickening, whereas the outer collagenous layer of Bruch's membrane appeared relatively normal. In addition, there was photoreceptor loss, disorganization of the RPE, and discontinuity and general thickening of Bruch's membrane. Electron microscopy of middle-aged retinas of both heterozygous and homozygous knock-in mice showed distinct abnormalities in the RPE, specifically affecting the thickness and organization of the basal microvilli. At this age, no abnormalities of Bruch's membrane comparable to those seen in late-stage human disease were noted. At 30 months of age, however, mutant (heterozygous and homozygous) animals showed more pronounced changes accentuated by increased thickening of Bruch's membrane and marked disturbances of the inner collagenous layer. Moreover, in many areas, the basal membrane of the RPE assumed a blurry appearance accompanied by a complete breakdown of the microvilli labyrinth. In those areas, large caverns were forming in the soma of the RPE. It should be emphasized that the human SFD eyes available for examination are generally obtained from donors of advanced age and with a long-time history of disease, making it difficult, if not impossible, to distinguish between primary pathologic features and secondary changes. So far, pathologic features of early SFD have not been documented in humans. At 30 months of age, the mice are near the end of their life spans in captivity but may be manifesting only the early stages of disease. If this were the case, our findings in the knock-in mouse would imply

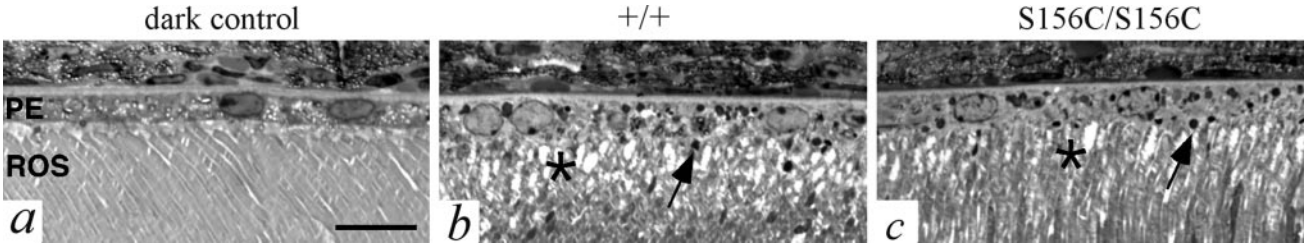

FIGURE 8. Disc shedding. Dark adapted wild-type (**a**, **b**) and age-matched *Timp3*$^{S156C/S156C}$ mice (**c**) were exposed to 13,000 lux of white light (**b**, **c**) or kept in darkness (**a**) as a control. After a recovery period of 90 minutes in darkness, retinas were analyzed. *Arrow*s: phagosomes; (*) dilated ROS. PE, pigment epithelium; ROS, rod outer segments. Bar, 10 μm.

that the primary site of SFD disease is at the junction of RPE and Bruch's membrane, with early manifestations in the basal labyrinth and disturbances in the inner collagenous layer of Bruch's membrane. Choroidal neovascularization and atrophic changes as seen in humans may then represent delayed reactions of the ECM–RPE disturbances that do not become manifest in the normal life span of the mouse.

Studies in both human and mouse have determined the RPE to be the site of normal *TIMP3* mRNA expression.[31–33] Furthermore, immunohistochemistry has localized the TIMP3 protein to Bruch's membrane in normal human eyes[33,34] and in the eyes of a donor with SFD.[3] Another report localized TIMP3 within Bruch's membrane but also at the level of the RPE, raising the additional possibility that the protein may also be secreted at the apical surface of the RPE cells.[35] Our immunofluorescence labeling studies in mouse retinal sections are in excellent agreement with the previous studies and show that Timp3 immunoreactivity is strongly associated with Bruch's membrane but also, to a minor extent, with the photoreceptor layer. The availability of the homozygous knock-in mouse provides the unique opportunity to analyze mutant Timp3 expression without the interference of cross-immunoreactivity to the normal protein. Our results show that mutant Timp3 localization within the retina is identical with that in wild-type retina. This strongly suggests that the Ser156Cys mutation does not influence site-specific binding to the extracellular matrix (i.e., Bruch's membrane), thus rejecting an earlier notion that a possible mechanism of disease may stem from an aberrant location of mutant Timp3.[33]

In an alternative hypothesis Langton et al.[11,16] suggest that an excess, rather than an absence or deficiency, of functional protein may underlay the pathogenesis of SFD. In a heterologous expression system, they have shown, in reverse zymogram assays, that mutant TIMP3 forms higher-molecular-weight complexes that retain an inhibitory effect on MMPs.[11,16] According to the model, the functional higher-molecular-weight Timp3 complexes may be less prone to degradation and thus may accumulate in Bruch's membrane over time. Subsequently, proper ECM remodeling would probably be impaired, leading to the known findings in Bruch's membrane. Our results in the knock-in mice provide several lines of evidence supporting the proposed model. First, we show that, similar to normal Timp3, the mutant form is strongly associated with Bruch's membrane. From immunofluorescence labeling studies there is no indication that the mutant protein may be displaced within the retinal tissues. Second, the higher-molecular-weight complexes could indeed be of direct relevance to SFD pathogenesis, because these complexes are not only formed in ECM extracts of in vitro cultured fibroblasts but are also present in the murine eye. Third, although accurate quantification of normal and mutant Timp3 in Bruch's membrane is difficult, our results indicate that there may be a relative increase in Timp3 levels in the mutant eye, although these latter findings must be further substantiated. It is not clear at this point whether there is an upregulation of Timp3 expression on the transcript or protein level or whether the mutation is directly or indirectly involved in Timp3 stability and turnover rate. Last, our studies demonstrate that early signs of disease in the mouse are exclusively found in cellular and extracellular structures tightly associated with mutant Timp3 localization, further supporting a direct role of the mutant protein in primary changes at the level of Bruch's membrane and the RPE.

We further used the mouse model to explore whether mutant Timp3 directly or indirectly increases the rate of cell death in the retina in response to light exposure. One possible mechanism is induction of apoptosis. TIMP3 has been shown to activate cell death in carcinoma cell lines,[36] and its overexpression promotes apoptosis in smooth muscle cells.[37] This activity has been localized to the N terminus of the protein and appears to be dependent on inhibition of MMP.[38] Examination of susceptibility to light damage revealed no difference between the retinas of wild-type and homozygous mutant mice. Retinal light damage is influenced by the chromophore rhodopsin, which controls photon absorption.[39] The rate of regeneration after bleaching is a major determinant of the susceptibility to light damage[28] and has been found to be abnormal in at least one patient with SFD.[40] Metabolic rhodopsin regeneration remained uninfluenced by the *Timp3* mutation in our mouse model. This is consistent with the observation of normal levels of the retinal proteins RPE65 and CRALBP as well as IRBP, which is expressed in the ECM. In addition, mutant mice showed similar levels of arrestin, which is involved in phototransduction. Exposure to bright light not only induces photoreceptor apoptosis but also potentiates the shedding of ROS tips (shedding burst), which usually follows a circadian rhythm with its peak at the beginning of the light phase.[29] Shedding and phagocytosis of ROS tips by the cells of the RPE involves the ECM, and therefore could be affected by *Timp3* gene mutations; however, in the homozygous mutant mice, we found no abnormalities in these processes.

The generation of the *Timp3*^{S156C} mouse model promises to be a helpful tool to further investigate the primary mechanisms of SFD. It is interesting to note that the mutant mouse displays a less severe phenotype than do patients with SFD, although the abnormal murine Timp3 appears to have the same biochemical characteristics as the human protein. It is unlikely that TIMP3, which is highly conserved between human and mouse (96% amino acid sequence identity) displays functional differences in the two species. A minor phenotype in the mouse may, however, be caused by a greater developmental plasticity in the mouse eye or by other adaptive mechanisms capable of compensating the deleterious effects of the introduced mutation. Examples illustrating such compensatory mechanisms are scarce in the literature but have been documented.[41–43] Alternatively, the development of pathologic features may be influenced by the genetic background and may require intervention strategies for the symptoms to manifest.[44] In fact, the observation that vitamin A supplementation reverses the night blindness in patients with SFD suggests that nutritional factors may affect SFD pathophysiology.[13] To this end, we have initiated long-term studies challenging the *Timp3* knock-in mice by vitamin A depletion. Similarly, isogenic breeding of the *Timp3* knock-in mutation onto defined mouse backgrounds may produce a more severe phenotype, possibly expressing the typical secondary manifestations of SFD, such as subretinal neovascularization and atrophy of the choriocapillaris.

Acknowledgments

The authors thank Andrea Gehrig for performing the Northern blot analyses, Birgit Geis for technical help with Western blot experiments, Gudrun Haerer for expert help with the electron microscopy, Ralf Tornow for help with the SLO imaging, Renate Mielke for technical assistance, and Werner Müller and Klaus Rajewsky for the LoxP and Cre plasmids.

References

1. Sorsby A, Mason MEJ, Gardner N. A fundus dystrophy with unusual features. *Br J Ophthalmol.* 1949;33:67–97.
2. Capon MRC, Marshall J, Krafft JI, Alexander RA, Hiscott PS, Bird AC. Sorsby's fundus dystrophy: a light and electron microscopic study. *Ophthalmology.* 1989;95:1769–1777.
3. Chong NHV, Alexander RA, Gin T, Bird AC, Luthert PJ. TIMP-3, collagen, and elastin immunohistochemistry and histopathology of

Sorsby's fundus dystrophy. *Invest Ophthalmol Vis Sci.* 2000;41: 898–902.
4. Klein R, Klein BE, Linton KL. Prevalence of age-related maculopathy: The Beaver Dam Eye Study. *Ophthalmology.* 1992; 99:933–943.
5. Weber BHF, Vogt G, Pruett RC, Stohr H, Felbor U. Mutations in the tissue inhibitor of metalloproteinases-3 (TIMP3) in patients with Sorsby's fundus dystrophy. *Nat Genet.* 1994;8:352–356.
6. Murphy G, Willenbrock F, Crabbe T, et al. Regulation of matrix metalloproteinase activity. *Ann NY Acad Sci.* 1994;732:31–41.
7. Loechel F, Fox JW, Murphy G, Albrechtsen R, Wewer UM. ADAM 12-S cleaves IGFBP-3 and IGFBP-5 and is inhibited by TIMP-3. *Biochem Biophys Res Commun.* 2000;278:511–515.
8. Hashimoto G, Aoki T, Nakamura H, Tanzawa K, Okada Y. Inhibition of ADAMTS4 (aggrecanase-1) by tissue inhibitors of metalloproteinases (TIMP-1, 2, 3 and 4). *FEBS Lett.* 2001;494:192–195.
9. Matrisian LM. The matrix-degrading metalloproteinases. *Bioessays.* 1992;14:455–463.
10. Stone AL, Kroeger M, Sang QX. Structure-function analysis of the ADAM family of disintegrin-like and metalloproteinase-containing proteins (review). *J Protein Chem.* 1999;18:447–465.
11. Langton KP, Barker MD, McKie N. Localization of the functional domains of human tissue inhibitor of metalloproteinases-3 and the effects of a Sorsby's fundus dystrophy mutation. *J Biol Chem.* 1998;273:16778–16781.
12. Felbor U, Stohr H, Amann T, Schonherr U, Weber, BHF. A novel Ser156Cys mutation in the tissue inhibitor of metalloproteinases-3 (TIMP3) in Sorsby's fundus dystrophy with unusual clinical features. *Hum Mol Genet.* 1995;4:2415–2416.
13. Jacobson SG, Cideciyan AV, Regunath G, et al. Night blindness in Sorsby's fundus dystrophy reversed by vitamin A. *Nat Genet.* 1995;11:27–32.
14. Felbor U, Suvanto EA, Forsius HR, Eriksson AW, Weber BHF. Autosomal recessive Sorsby fundus dystrophy revisited: molecular evidence for dominant inheritance. *Am J Hum Genet.* 1997;60: 57–62.
15. Tabata Y, Isashiki Y, Kamimura K, Nakao K, Ohba N. A novel splice site mutation in the tissue inhibitor of the metalloproteinases-3 gene in Sorsby's fundus dystrophy with unusual clinical features. *Hum Genet.* 1998;103:179–182.
16. Langton KP, McKie N, Curtis A, et al. A novel tissue inhibitor of metalloproteinases-3 mutation reveals a common molecular phenotype in Sorsby's fundus dystrophy. *J Biol Chem.* 2000;275: 27027–27031.
17. Schrewe H, Gendron-Maguire M, Harbison ML, Gridley T. Mice homozygous for a null mutation of activin β_B are viable and fertile. *Mech Dev.* 1994;47:43–51.
18. Stohr H, Marquardt A, Rivera A, et al. A gene map of the Best's vitelliform macular dystrophy region on chromosome 11q12–q13.1. *Genome Res.* 1998;8:48–56.
19. Bradford MM. A rapid and sensitive method for the quantitation of microgram quantities of protein utilizing the principle of protein-dye binding. *Anal Biochem.* 1976;72:248–254.
20. Redmond TM, Hamel CP. Genetic analysis of RPE65: from human disease to mouse model. *Methods Enzymol.* 2000;316:705–724.
21. Smith SB, McClung J, Wiggert BN, Nir I. Delayed rhodopsin regeneration and altered distribution of interphotoreceptor retinoid binding protein (IRBP) in the mi(vit)/mi(vit) (vitiligo) mouse. *J Neurocytol.* 1997;26:605–613.
22. Crabb JW, Gaur VP, Garwin GG, et al. Topological and epitope mapping of the cellular retinaldehyde-binding protein from retina. *J Biol Chem.* 1991;266:16674–16683.
23. Kueng-Hitz N, Grimm C, Lansel N, et al. The retina of c-*fos*$^{-/-}$ mice: electrophysiologic, morphologic and biochemical aspects. *Invest Ophthalmol Vis Sci.* 2000;41:909–916.
24. Seeliger MW, Narfström K, Reinhard J, Zrenner E, Sutter E. Continuous monitoring of the stimulated area in multifocal ERG. *Doc Ophthalmol.* 2000;100:167–184.
25. Jaissle G, May CA, Reinhard J, et al. Evaluation of the rhodopsin knockout mouse as a model of pure cone function. *Invest Ophthalmol Vis Sci.* 2001;42:506–513.
26. Seeliger MW, Grimm C, Ståhlberg F, et al. New views on RPE65 deficiency: the rod system is the source of vision in a mouse model of Leber congenital amaurosis. *Nat Genet.* 2001;29:70–74.
27. Zeng Y, Rosborough RC, Li Y, Gupta AR, Bennett J. Temporal and spatial regulation of gene expression mediated by the promoter for the human tissue inhibitor of metalloproteinases-3 (TIMP-3)-encoding gene. *Dev Dyn.* 1998;211:228–237.
28. Wenzel A, Remé CE, Williams TP, Hafezi F, Grimm C. The Rpe65 Leu450Met mutation increases retinal resistance against light-induced degeneration by slowing rhodopsin regeneration. *J Neurosci.* 2001;21:53–58.
29. Reme CE, Braschler U, Wirz-Justice A, Munz K. Disk-shedding in the rat retina: lithium dampens the circadian rhythm but potentiates the light response. *Brain Res.* 1990;523:167–170.
30. Ashton N, Sorsby A. A fundus dystrophy with unusual features: a histological study. *Br J Ophthalmol.* 1951;35:751–764.
31. Della NG, Campochiaro PA, Zack DJ. Localization of TIMP-3 mRNA expression to the retinal pigment epithelium. *Invest Ophthalmol Vis Sci.* 1996;37:1921–1924.
32. Ruiz A, Brett P, Bok D. TIMP-3 is expressed in the human retinal pigment epithelium. *Biochem Biophys Res Commun.* 1996;226: 467–474.
33. Vranka JA, Johnson E, Zhu X, et al. Discrete expression and distribution pattern of TIMP-3 in the human retina and choroid. *Curr Eye Res.* 1997;16:102–110.
34. Fariss RN, Apte SS, Olsen BR, Iwata K, Milam AH. Tissue inhibitor of metalloproteinases-3 is a component of Bruch's membrane of the eye. *Am J Pathol.* 1997;150:323–328.
35. Jomary C, Neal MJ, Iwata K, Jones SE. Localization of tissue inhibitor of metalloproteinases-3 in neurodegenerative retinal disease. *Neuroreport.* 1997;8:2169–2172.
36. Baker AH, George SJ, Zaltsman AB, Murphy G, Newby AC. Inhibition of invasion and induction of apoptotic cell death of cancer cell lines by overexpression of TIMP-3. *Br J Cancer.* 1999;79:1347–1355.
37. Baker AH, Zaltsman AB, George SJ, Newby AC. Divergent effects of tissue inhibitor of metalloproteinases-1, -2, or -3 overexpression on rat vascular smooth muscle cell invasion, proliferation, and death in vitro: TIMP-3 promotes apoptosis. *J Clin Invest.* 1998;101: 1478–1487.
38. Bond M, Murphy G, Bennett MR, et al. Localization of the death domain of tissue inhibitor of metalloproteinase-3 to the N terminus. *J Biol Chem.* 2000;275:41358–41363.
39. Grimm C, Wenzel A, Hafezi F, Yu S, Redmond TM, Reme CE. Protection of Rpe65-deficient mice identifies rhodopsin as a mediator of light-induced retinal degeneration. *Nat Genet.* 2000;25: 63–66.
40. Steinmetz RL, Polkinghorne PC, Fitzke FW, Kemp CM, Bird AC. Abnormal dark adaptation and rhodopsin kinetics in Sorsby's fundus dystrophy. *Invest Ophthalmol Vis Sci.* 1992;33:1633–1636.
41. Tunstall AM, Merriman JM, Milne I, James K. Normal and pathological serum levels of alpha2-macroglobulins in men and mice. *J Clin Pathol.* 1975;28:133–139.
42. Himms-Hagen J. Physiological roles of the leptin endocrine system: differences between mice and humans. *Crit Rev Clin Lab Sci.* 1999;36:575–655.
43. Gödecke A, Flogel U, Zanger K, et al. Disruption of myoglobin in mice induces multiple compensatory mechanisms. *Proc Natl Acad Sci USA.* 1999;96:10495–10500.
44. Mackie EJ, Tucker RP. The tenascin-C knockout revisited. *J Cell Sci.* 1999;112:3847–3853.